SAXS and TEM Studies on Poly(styrene)-*block*-poly(ethene-*co*-but-1-ene)-*block*-poly(styrene) in Bulk and at Various Interfaces

Barbara Heck,[†] Peter Arends,[‡] Markus Ganter,[‡] Jörg Kressler,*[,‡] and Bernd Stühn*[,†]

Fakultät für Physik and Institut für Makromolekulare Chemie und Freiburger Materialforschungszentrum, Albert-Ludwigs-Universität Freiburg, Stefan-Meier-Strasse 21, D-79104 Freiburg i. Br., Germany

Received November 19, 1996; Revised Manuscript Received May 21, 1997[⊗]

ABSTRACT: SAXS and TEM measurements are employed in order to study the morphology of poly(styrene)-*block*-poly(ethene-*co*-but-1-ene)-*block*-poly(styrene) (SEBS) with 29 wt % styrene (Kraton G1652) in bulk and at interfaces to different polymers. Temperature-dependent SAXS measurements of the SEBS bulk sample reveal that PS cylinders are hexagonally packed in the EB matrix. The lattice constant increases during cooling from 200 to 120 °C from 27.5 to 29.5 nm and simultaneously an increase of the cylinder radius occurs from 7 to 7.5 nm. The lattice constant obtained by SAXS is in agreement with TEM measurements on ultrathin sections of the bulk sample. TEM tilting experiments confirm the existence of cylindrical microdomains in the SEBS bulk phase. Furthermore, the behavior of SEBS at the interface with various polymers is studied by TEM and peel tests. TEM measurements show that SEBS forms one lamella at the interface PS homopolymer having a molecular weight much larger than the PS blocks. This results only in a very weak adhesion between SEBS and PS homopolymer measured by a peel test using bilayer specimens. In contrast there is a strong adhesion at the interface of SEBS with poly(3,5-dimethylphenylene ether) (PPE) or isotactic polypropylene (i-PP) after thermal annealing. This can be explained by the miscibility of the PS blocks with PPE and of the EB matrix of the block copolymer with i-PP, respectively. This leads to interfacial phase transitions, to cooperative orientation processes of PS cylinders, and finally to diffusion processes of disordered micelles as verified by TEM micrographs.

Introduction

The triblock copolymer poly(styrene)-*block*-poly(ethene-*co*-but-1-ene)-*block*-poly(styrene) (SEBS) with PS contents typically in the range between 20 and 35 wt % is a thermoplastic elastomer.[1] SEBS is obtained by hydrogenation of triblock copolymers of styrene and butadiene (SBS). Because of the commercial production of SEBS or triblock copolymers of styrene and isoprene (SIS), these materials are widely used for the modification and compatibilization of polymer blends.[2] First morphological studies showed that these types of triblock copolymers with sufficiently high molecular weights form ordered microphases governed on composition.[3] Solvent cast films may form depending on the nature of the solvent spherical, cylindrical, or lamellar morphologies for an identical triblock copolymer.[3] It is generally assumed that triblock copolymers of the type ABA generate morphologies similar to those for diblock copolymers. There has been only one report on a hexagonal arrangement of ellipsoids for SBS with 26.5 vol % of PS, which is not known for diblock copolymers.[4] But it has been shown recently that a number of microdomain arrangements might be stable at intermediate composition ranges between lamella/cylinder and cylinder/sphere transitions.[5] Furthermore, extensive studies have shown that symmetric block copolymers show ordering phenomena near to free surfaces or interfaces, i.e. lamellae orient parallel to the block copolymer surface driven by differences of the surface tension of the respective blocks (see ref 6 and references therein). Studies on the ordering behavior of asymmetric block copolymers are rather limited. One study was able to show that triblock copolymers of poly(styrene) and poly(vinylpyridine) (PVP) with a cylindrical morphology show a better ordering of cylinders parallel to the surface of silicon wafers than the respective diblock copolymer with the same morphology.[7] Also an interfacial phase transition from cylindrical to lamellar morphology could be observed as theoretically predicted.[8]

The aim of this study is to confirm the arrangement of microdomains of an SEBS triblock copolymer with 29 wt % PS in the bulk by transmission electron microscopy (TEM) and small-angle X-ray scattering (SAXS). Then we focus on the behavior of SEBS at various polymeric interfaces studied by TEM and peel tests. Therefore, bilayer specimens of SEBS with isotactic polypropylene (i-PP), with atactic polystyrene (a-PS), or with poly(3,5-dimethylphenylene ether) (PPE) have been prepared.

Experimental Section

Materials. The polymers used and their characteristic data are summarized in Table 1.

SAXS. The SEBS block copolymer was placed in an evacuated tool and heated to 220 °C. It was then pressed to yield a homogeneous block of 2 mm thickness. The sample was cooled to room temperature and placed in a brass sample holder. During the SAXS experiments it was kept in an evacuated Kratky compact camera (PAAR, Graz, Austria). The scattering experiments use the radiation from a sealed X-ray tube with copper anode and a Siemens generator (Kristalloflex 710H). A primary monochromator selects the wavelength of *Cu Kα* of $\lambda = 0.154$ nm. The accessible range of scattering vectors $q = (4\pi/\lambda)\sin(\theta/2)$ is $0.1 < q/\mathrm{nm}^{-1} < 5$, where θ is the scattering angle. The scattered intensity is recorded with a scintillation counter in step scanning mode, and the average

[†] Fakultät für Physik.
[‡] Institut für Makromolekulare Chemie und Freiburger Materialforschungszentrum.
[⊗] Abstract published in *Advance ACS Abstracts,* July 15, 1997.

S0024-9297(96)01707-X CCC: $14.00

Table 1. Molecular Weights, Glass Transitions, and Sources of Polymers Used

polymer	M_w	M_w/M_n	T_g (°C)	source
SEBS[a]	87 000	1.04		Shell
S blocks	2 × 12 600		83	KratonG1652
EB block[b]	61 800		−49	
a-PS	158 000	2.0	100	BASF
i-PP	46 500	7.6	1	Shell KM6100
PPE	53 000	2.0	215	BASF

[a] Contains 29 wt % PS. [b] The polybutadiene precursor of the olefinic block had 40% 1,2 and 60% 1,4 modes of enchainment.

time to obtain a scattering profile is 2 h. Due to the slitlike cross section of the primary beam in this set up, the scattered intensity at one angle contains a certain range of scattering vectors. This problem is solved by desmearing the data using standard methods.[9] Moreover the data are put on an absolute scale using the moving slit device (PAAR) to determine the flux of the primary beam. The resulting intensity is the scattering cross section per volume in units of the Thompson cross section.

TEM. Most of the TEM measurements were carried out with a Zeiss CEM 902 transmission electron microscope applying an acceleration voltage of 80 keV. The specimens were cut by an ultramicrotome (Ultracut E, Reichert & Jung) equipped with a diamond knife. Ultrathin sections of approximately 50 nm thickness were stained in the RuO_4 gas phase, i.e. the PS blocks are stained selectively.[10] For tilting experiments, a LEO 912 Omega with an acceleration voltage of 120 keV, equipped with a goniometer, was used.

Peel Test. For each polymer, plates of 2 mm thickness were pressed under vacuum at 240 °C. Typically the polymers were isothermally annealed for 10−15 min and then pressed for only 30 s with 30 bar in order to prevent major orientation processes during the sample preparation. Furthermore, the samples were always pressed between Kapton sheets. Bars with dimensions of 50 × 9 × 2 mm were cut out of the plates. Bilayer specimens were prepared by mounting the bars of each polymer together. A distance holder of 3.7 mm was used to prevent the block copolymer from deforming during pressing. Silicone sheets above and below the specimen ensured a uniform pressure. The polymers were kept isothermally pressed on each other for various times. These specimens were partially separated at the interface using a razor blade. The SEBS layer was bent and fixed in the Instron 4204 machine.[11] The cross head speed was 10 mm/min. The force necessary to separate the two layers was measured. The average delamination force was normalized by the width of the specimen to calculate the peel strength.

Results and Discussion

SEBS in Bulk. In order to obtain information on the size and the spatial arrangement of the microdomains, SAXS measurements were carried out in the range between room temperature and 220 °C. The sample was slowly heated to 220 °C. The data were taken at fixed temperature, and the sample was annealed after each cooling step for a minimum of 30 min. The scattering pattern for all temperatures showed several maxima, indicating the existence of an ordered structure as is to be expected for this molecular weight.[12] A typical example of these measurements taken at 120 °C is displayed in Figure 1. Three maxima are clearly discernible in this diagram. Closer inspection reveals that the second and third maxima are composed of several reflections. If we denote the q position of the first maximum by q^* then higher order reflections are found at multiples of $\sqrt{3}$, $\sqrt{4}$, $\sqrt{7}$, and $\sqrt{9}$. This sequence of reflections is in accordance with the assumption of a hexagonal packing of cylinders (hpc). In

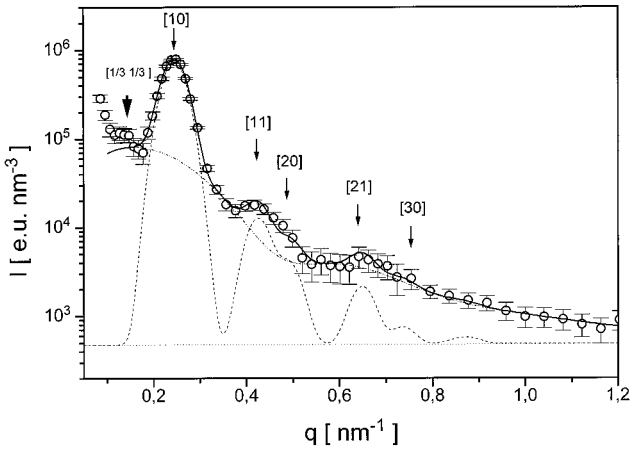

Figure 1. SAXS trace of SEBS taken at 120 °C. The circles represent the desmeared and corrected data; the full line represents the best fit summarizing all contributions of the density fluctuations (dotted line), the diffuse scattering (dashed−dotted line), and Bragg reflections (dashed line).

the following we aim at a quantitative description of the scattering profile in order to extract precise information on the microdomain size and the lattice parameters using a method described elsewhere.[13] We treat the sample as an arrangement of crystalline grains without any preferred orientation. It is therefore analogous to a polycrystalline powder sample. The assignment of the scattering maxima to Bragg reflections from the hexagonal lattice is also given in Figure 1. All peaks may be assigned to the reflections of a two dimensional hexagonal lattice with Miller indices hk. Consequently no information on a possible structure along the cylinder axis may be derived from the Bragg reflections. The scattered intensity of the Bragg reflections at scattering vector q in an isotropic sample is given as

$$I_{\text{Bragg}}(q) = \sum \bar{\phi}^2(q_{hk}) \frac{j_{hk}}{q^2} G_{hk}(q;\sigma) \exp\{-q_{hk}{}^2 u^2/3\} \quad (1)$$

Equation 1 contains a Lorentz factor $1/q^2$ for an isotropic distribution of grains. The sum is over all groups of reflections $\{hk\}$. j_{hk} is the multiplicity of reflection $\{hk\}$ and $G_{hk}(q;\sigma)$ denotes a normalized Gaussian centered at q_{hk} with a variance of σ. The peak position q_{hk} is directly related to the lattice constant and intercylinder distance a

$$q_{hk} = \frac{2\pi}{a}\sqrt{\frac{4}{3}(h^2 + k^2 + hk)} \quad (2)$$

In particular we have $q^* = q_{100} = 4\pi/a\sqrt{3}$.

The modulating factor in the intensity of a reflection is the form factor of the scattering particle, which in the present case is the cylinder consisting of poly(styrene). The scattering from a cylindrical particle with radius R and length L has been discussed in ref 14. Let α denote the angle between the cylinder axis and the scattering vector $\vec{q}$ then the scattering amplitude $\phi(q)$ of a cylindrical particle is

$$\phi(q) = 2V \frac{\sin\left(\frac{qL}{2}\cos\alpha\right)}{\frac{qL}{2}\cos\alpha} \frac{J_1(qR\sin\alpha)}{qR\sin\alpha} \quad (3)$$

where V is the volume of a cylinder and J_1 is the first-order Bessel function. For a given Bragg reflection at

q_{hk} it is convenient to introduce cylindrical coordinates and to decompose the scattering vector into its radial and z component $q_r = q \sin \alpha$ and $q_z = q \cos \alpha$, respectively. For the reflections present in our scattering profile, the scattering vector has only a q_r component with a length given by eq 2. From the Bragg intensities alone, we are therefore not able to determine the length of the cylinders L. It is to be expected that this parameter is not well defined anyway and the reciprocal space of the system is really two-dimensional.

The average in eq 1 is over the size distribution of the cylinder radii R. We perform this average numerically using a Gaussian distribution for R with a mean $\bar{R}$ and a variance σ_R. Other authors[15] extend eq 3 with an exponential to take the softness of the interface between the poly(styrene) cylinder and the EB matrix into account. We do not insist on this factor as it is difficult to discriminate it from the normal Debye–Waller factor which is present in eq 1. Both carry the same q dependence. The physical origin of the Debye–Waller factor is the deviation of the location of individual scatterers from their mean by a mean squared displacement u^2. It gives rise to a decrease of the peak intensities.

A second consequence of this type of lattice distortion is the presence of diffuse scattering I_{diff}. Due to the large size of the scattering particles, this scattering contribution shows a marked q dependence which may be exploited to obtain more information on the radii and the length of the cylinders.

If we assume the deviation of the local form factor of a cylinder to be uncorrelated, then

$$I_{diff} \propto (1 - \exp(-q^2u^2/3))(\overline{\phi^2} - \bar{\phi}^2) \qquad (4)$$

In order to simplify calculations we observe that averaging ϕ with respect to the size distribution will smear out its maxima, and we assume $I_{diff} \approx K_{diff}(1 - \exp(-q^2u^2/3))\overline{\phi^2}$ with K_{diff} an adjustable prefactor. The radius of the poly(styrene) cylinders enters the intensities of the Bragg reflections as well as the q dependence of the diffuse scattering. The additional average over all orientations of the cylinder axis of $\overline{\phi^2}$ is done numerically.[14]

A third contribution to the scattering I_κ arises from the density fluctuations and is taken into account as a constant. The scattered intensity is then given as

$$I(q) = I_{Bragg} + I_{diff} + I_\kappa \qquad (5)$$

Equation 5 is now fitted to the experimental data in a least-squares procedure, and the result for $T = 120$ °C is shown in Figure 1 as the full line. The model obviously provides a very good fit to the data. In order to discriminate the three components of the scattered intensity, they are included in Figure 1 as the broken lines. The intercylinder distance is found to be $a = 29.54$ (± 0.03) nm, and the cylinder radius $\bar{R} = 7.5$ (± 0.1) nm. The distribution of radii is characterized by a variance $\sigma_R = 1.4$ nm independent of T. The width of the Bragg reflections is $\sigma = 0.03$ nm^{-1}.

In the hpc structure every plane perpendicular to the cylinder axis must show a surface coverage with cylinder cross section which is identical to the volume fraction of the cylinders f. We can calculate f from the dimensional parameters as $f = 2\pi/\sqrt{3}(R/a)^2$ and arrive at $f = 0.23$. This value agrees fairly well with the poly(styrene) volume fraction of SEBS (0.25).

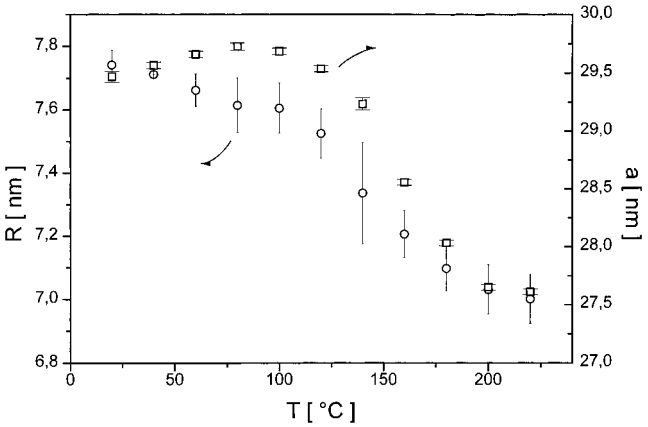

Figure 2. Cylinder radius R and lattice constant a of SEBS as a function of temperature.

Turning to the temperature dependence of the structure, we observe that the model as discussed above describes very well the temperature range from $T = 120$ up to 220 °C. At lower temperature we find clear deviations between the data and the hpc model in particular in the regime of the {21} and the {30} reflections. We were not able to describe these deviations quantitatively as a modification of the particle scattering factor. Therefore, the hpc model is used in the full range of temperatures. As a result, we are now able to determine the cylinder radius and the cylinder distance in dependence on temperature. These data are displayed in Figure 2. We observe that both quantities increase with decreasing temperature by nearly 10%. The lattice cell expands laterally, but the surface coverage and therefore f remains essentially constant. The structure shrinks in the direction of the cylinder axis.

A closer look at the temperature dependence of a and R suggests these changes to take place in a well-defined temperature regime and to saturate below 90 °C. This coincides with the glass transition temperature of the poly(styrene) domains (83 °C) which may be responsible for the stopping of the structural changes with decreasing T. An important conclusion is, however, that deviations from the well-defined hpc structure are observed below 120 °C.

As a final observation deduced from SAXS data, we point to the small peak at small angles which is marked by a bold arrow in Figure 1. It is clearly present in the scattering profiles below 120 °C. Its q position shifts with T in accordance with the other reflections of the profile. Within the hpc lattice cell it is indexed as ($^1/_3$, $^1/_3$) and is consequently taken as an indication for superstructure formation within the lateral plane.

TEM is able to provide more local information in selected areas of block copolymers (usually in the range of a few square micrometers) in contrast to SAXS measurements which probe a large sample volume. Figure 3 shows three representative TEM micrographs of neat SEBS taken at arbitrarily chosen directions of microtoming of a bulk sample. The PS microdomains appear dark, caused by the RuO_4 staining, and the EB matrix is bright. It can be seen that the SAXS data treatment similar to that of a polycrystalline powder is justified. Crystalline grains without any preferred orientation can be distinguished clearly. These photographs are in agreement with the hpc microdomain arrangement obtained by SAXS. This can be seen better in Figure 4 which depicts schematically the hpc ar-

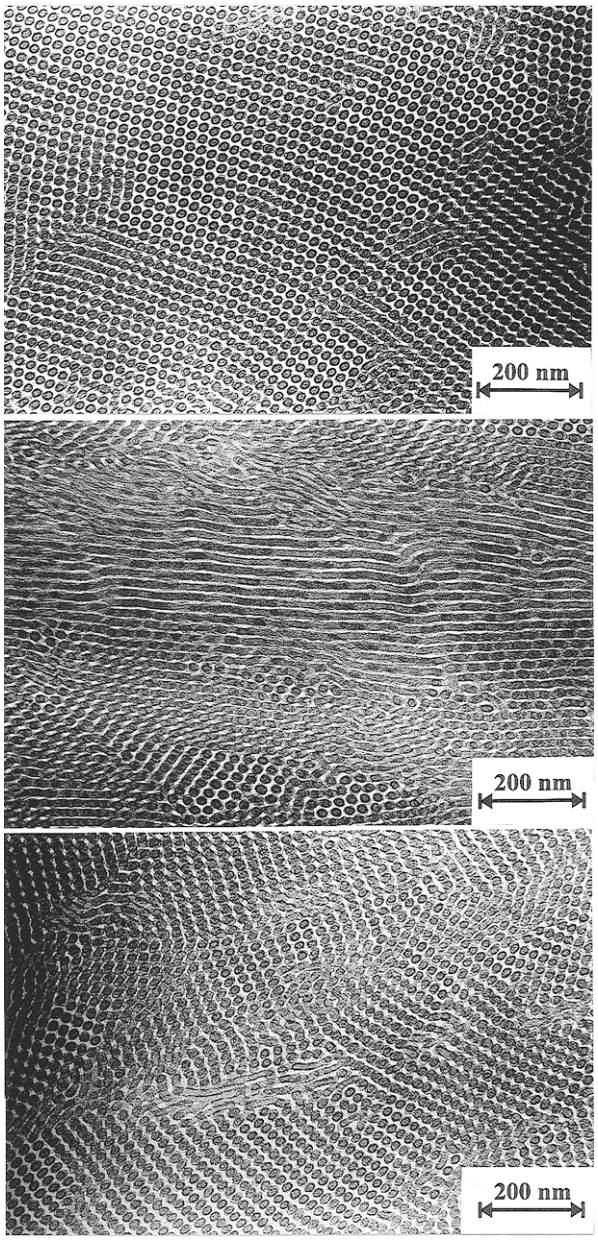

Figure 3. Three typical TEM micrographs of ultrathin sections of an SEBS bulk sample. The PS domains appear dark caused by the RuO_4 staining.

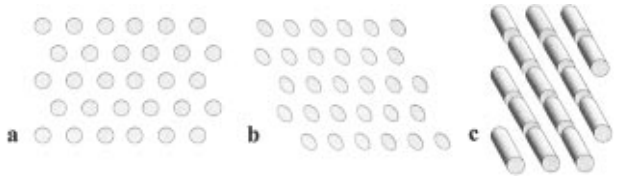

Figure 4. Simulation of TEM micrographs assuming an hpc arrangement of PS domains in an EB matrix and $a = 4R$: (a) cylinders truncated exactly perpendicular to their long axis; (b) truncated cylinders which were tilted; (c) cylinders truncated along their axis.

rangement observed by TEM. Figure 4a shows schematically the hexagonal arrangement of cylinders truncated exactly perpendicular to the cylinder axis. This leads to the classical hexagonal arrangement in the two-dimensional plane. This morphology can also be seen in the upper photograph of Figure 3. In Figure 4, the ratio of cylinder radius to lattice constant (approximately 1:4), obtained by SAXS, is used. Slightly tilting these cylinders and assuming the same direction of truncation lead to apparent ellipsoids (see Figure 4b) frequently observed in the TEM image (see e.g. bottom photograph in Figure 3). Moreover, the lattice appears to be distorted, which is only a microtoming effect. An apparently lamellar morphology is observed in the middle part of Figure 3. This morphology can also be explained with an hpc geometry as shown in Figure 4c. Microtoming the cylinders along their axis yields this arrangement. This can also be observed in the case that not all cylinders are cut exactly along their axis. Then several dots will appear in the apparent lamellae at places where the cylinders have an overlap. A necessary condition for the formation of apparent lamellae is that the length of cylinders is at least larger than the lattice constant a. The lattice constant a is also measured from several TEM micrographs where the cylinders are truncated exactly perpendicular to their axis (more than 10 photographs are taken). The average value obtained from TEM is 28.6 nm. This is in very good agreement with the SAXS value of about 29.5 nm. A clear disagreement occurs between the cylinder diameters obtained by TEM and SAXS. The cylinder diameter obtained by TEM is always larger compared to the SAXS value. It becomes obvious when comparing the simulations of TEM micrographs which use the SAXS data with the real TEM micrographs. The lower photograph of Figure 3 shows some rows of parallel ellipsoids. Comparing this photograph with the simulation in Figure 4b leads to a clear disagreement. The ellipsoids can only be formed by cylinders which are not truncated exactly perpendicular to the cylinder axis as already discussed. It is furthermore clear that the cylinders must be tilted in the direction of the long axis of the ellipsoids. Thus it is possible to observe rows of ellipsoids as can be seen from the simulation in Figure 4b. But recalling the SAXS results that a is about $4R$ as shown in the previous section makes clear that the distance between the neighboring ellipsoids in one row is not large enough. In the TEM micrographs they nearly touch each other. This behavior might be caused by different reasons. The staining procedure may deposit an excess of RuO_4 to the cylinders so that they appear too large. The photographs always show that the cylinders are darker at the interface PS cylinder/EB matrix compared to the center. This again can be a staining artifact or may be caused by a lower density in the cylinder/matrix interface which makes a penetration of this area with RuO_4 more likely. Furthermore, the SAXS data indicate a clear increase of the cylinder diameter with decreasing temperature. This process stops in the range of the glass transition of the PS blocks. It might be possible that this process continues in the ultrathin sections which were kept for a long time at room temperature, which is well above the glass transition of the EB block.

It has been shown that all morphologies observed by TEM can be explained with the hpc model. But the TEM photographs shown above do not show long cylinders directly. In order to exclude completely that microdomains as spheres or ellipsoids are present (which might generate under certain truncation conditions very similar TEM images), it is relevant to carry out tilting experiments by TEM as shown in Figure 5. Figure 5a,b shows SEBS at the interface to i-PP. The behavior of SEBS at the interface to i-PP will be discussed below. The interfacial area of SEBS is chosen in order to have some characteristic structures to ensure that exactly the same spot is observed in the tilting

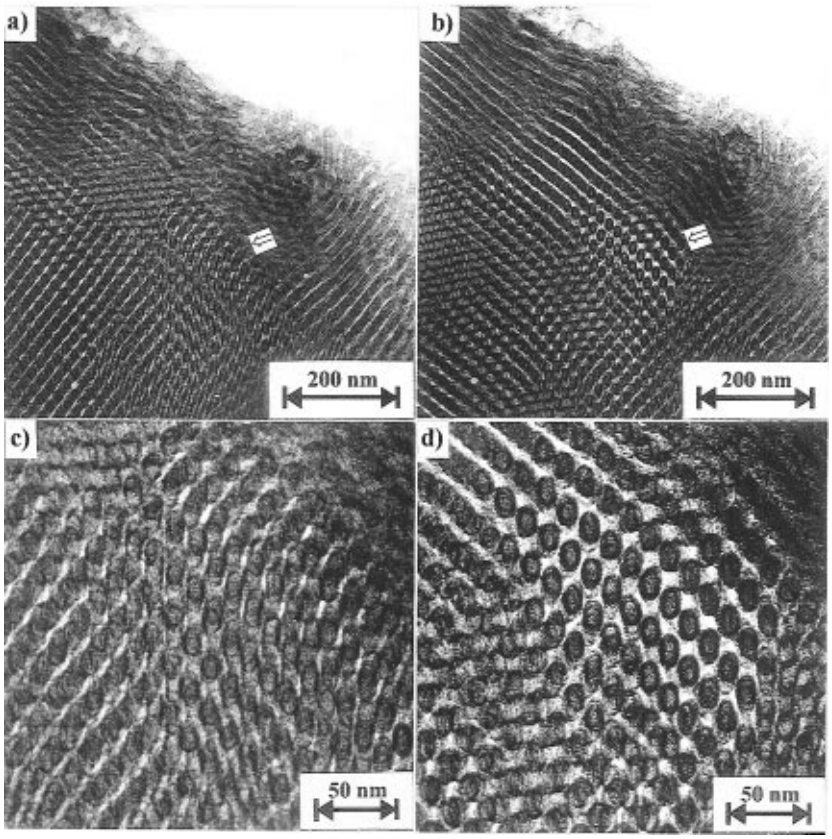

Figure 5. TEM micrographs of SEBS at the interface with i-PP. Parts a and b show an overview of an identical area observed at different angles (tilted −6° and +6°, respectively). The arrows indicate areas shown enlarged in parts c and d.

experiments. It can be seen that parts a and b of Figure 5 show exactly the same area of the sample. Figure 5a shows a TEM micrograph of a sample tilted by −6° with respect to the plane perpendicular to the electron beam, and Figure 5b shows the same sample tilted by +6°. Figure 5d shows the enlarged area indicated by an arrow in Figure 5b. Single ellipsoids can be seen clearly. In contrast the same area observed with a difference of 12° does not allow the observation of separate ellipsoids (Figure 5c). This is a clear indication for elongated microdomains as cylinders, at least over a length equal to the thickness of the ultrathin section (approximately 50 nm).

SEBS at Various Interfaces. As already mentioned, SEBS is frequently used for the compatibilization of immiscible polymer blends. Therefore, it is important to understand the behavior of SEBS at polymeric interfaces. Recently we reported the first results on the behavior of SEBS at the interface with i-PP.[11] Figure 6 shows SEBS at the interface to a-PS after an annealing time of 23.3 h at 170 °C. The left part represents the microphase-separated SEBS and the right part is a-PS homopolymer. It can be seen that SEBS is widely unaffected by the presence of a-PS. The dark stripe at the interface might be caused by the formation of an interfacial lamella. This behavior has been known from a triblock copolymer of PS and PVP which also forms at the surface a lamella though the bulk morphology is cylindrical.[7] Ordering phenomena in the SEBS phase cannot be observed unambiguously because the ultrathin sections are too thick. This sample is extremely difficult to handle because during the microtoming it fails frequently at the interface, and thus sections thicker than 100 nm had to be prepared. Also results of the peel test, as discussed below, indicate that there is only a very weak adhesion between the

Figure 6. TEM micrograph of SEBS at the interface to PS after an isothermal annealing at 170 °C for 23.3 h.

PS block and the PS homopolymer. This is reasonable because the PS hompolymer has a much larger molecular weight compared to the PS block. It has been known that in the case of a blend of hompolymer A with a block copolymer of type AB miscibility occurs only in the case that A has a lower molecular weight than the block A caused by entropic restrictions.[16] It should be mentioned that the situation is slightly more compli-

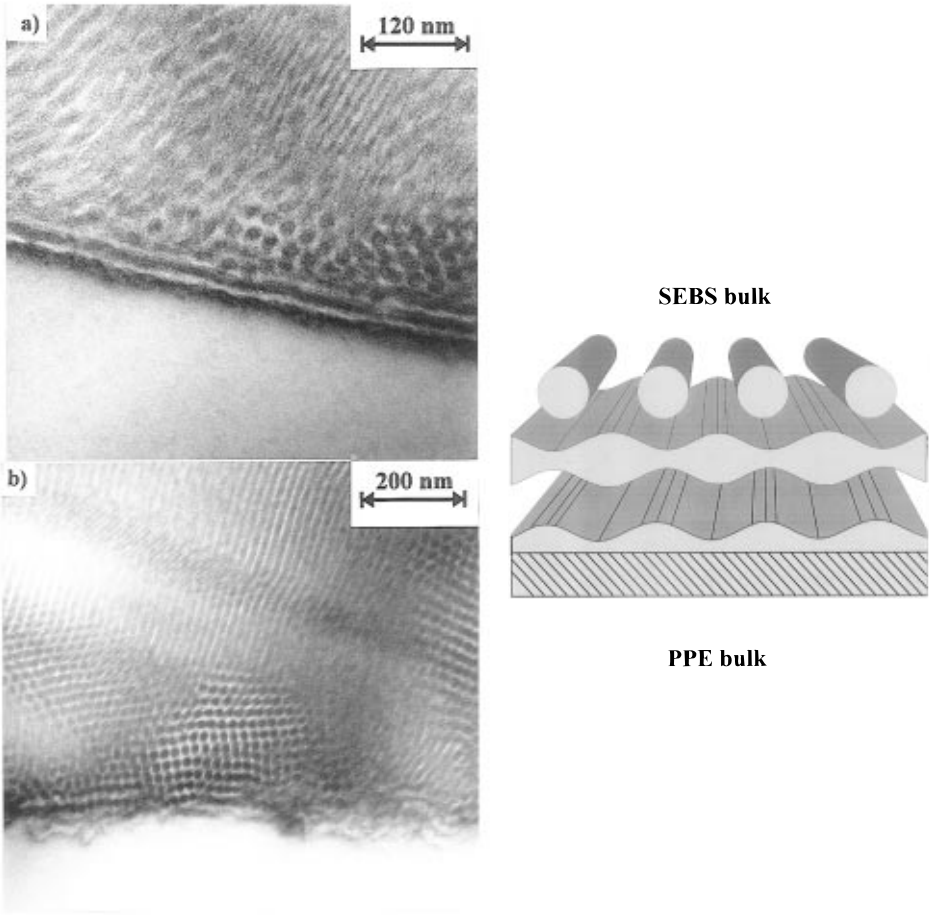

Figure 7. TEM micrograph of SEBS at the interface to PPE after isothermal annealing at 225 °C: (a) annealing for 15.25 h; (b) annealing for 38.8 h; (c) schematic drawing of the behavior of SEBS at the interface to PPE.

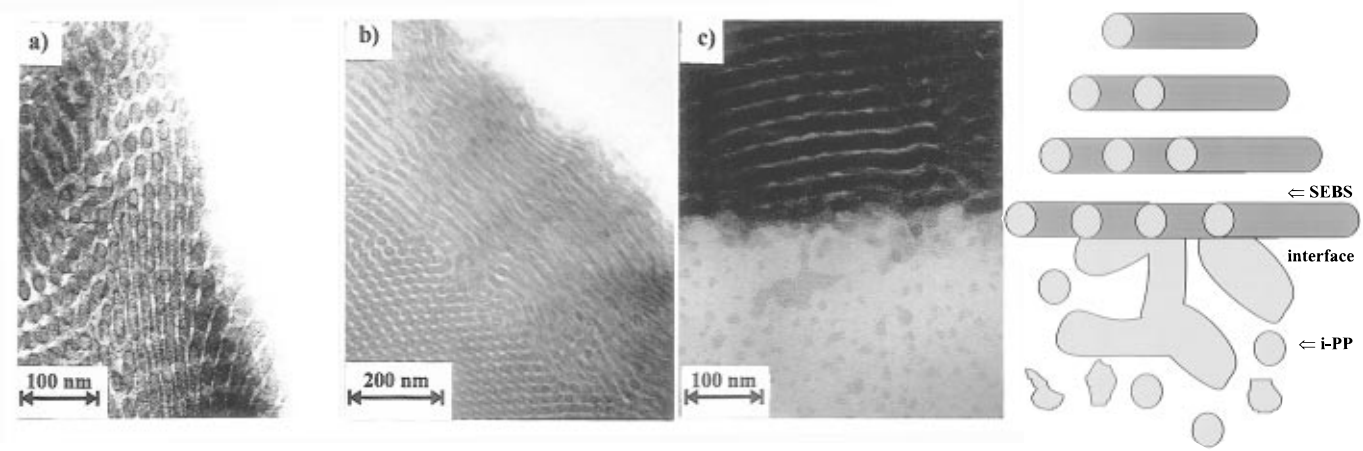

Figure 8. (a−c) TEM micrographs of SEBS at the interface to i-PP after an isothermal annealing at 165 °C for 2 h taken at different areas. (d) Schematic representation of the behavior of PS cylinders at the interface with i-PP.

cated because it depends on whether block A is the continuous or dispersed phase. However, the TEM micrograph indicates definitively that a long-range interdiffusion between the SEBS and PS homopolymer does not occur.

Figure 7 shows a different situation for bilayer specimens of SEBS and PPE. It has been known that PPE is miscible with a-PS caused by strong attractive interactions ($\chi_{PPE/PS} = -0.1$).[17] These favorable enthalpic interactions are also responsible for the miscibility of PPE with PS in block copolymers even in the case where PPE has a much larger molecular weight than the PS block.[18−20] The question remains as to how PPE influences SEBS when there is an interfacial contact. Figure 7a shows a TEM micrograph of the SEBS / PPE interface after isothermal annealing for 15.25 h at 225 °C. This temperature is very close to the glass transition of PPE at about 215 °C. Therefore, diffusion processes and ordering phenomena take place reasonably slow and can be studied time resolved. Obviously, a conversion of cylinders to lamellae occurs at the interface as schematically depicted in Figure 7c. This can be considered as an interfacial phase transition. At first the PS cylinders orient parallel to the PPE surface. When PS cylinders are in contact with the PPE surface, they start to spread and form a lamella. The driving force for these processes is the strong attractive interactions between PS and PPE. Again this behavior is

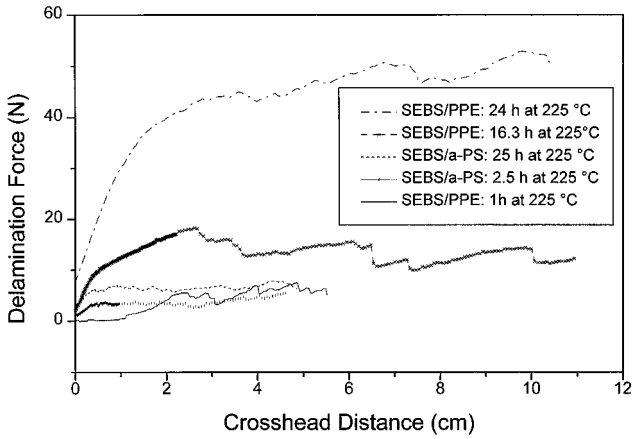

Figure 9. Crosshead distance vs delamination force of the peel test of bilayer specimens of SEBS/PPE and SEBS/a-PS after different annealing times at 225 °C. The traces from the bottom to the top were obtained with samples of widths of 9.9, 9.7, 10.2, 9.6, and 11.0 mm.

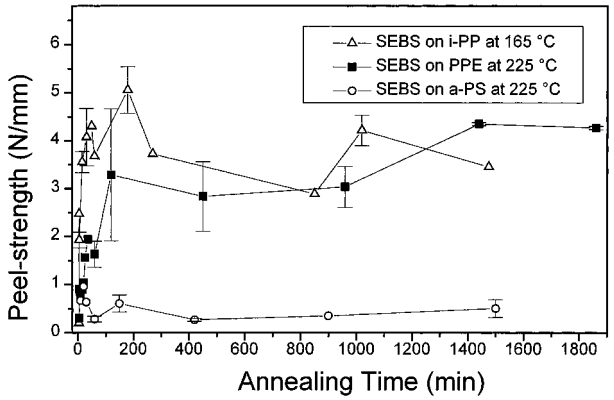

Figure 10. Peel strength as a function of annealing time for SEBS on three different polymers.

similar to other experimental findings and theoretical predictions for free block copolymer surfaces.[7,8] After a longer annealing time of 38.8 h at 225 °C the lamellae start to dissolve caused by the excess of PPE (Figure 7b). The lamellae do not dissolve regularly; i.e., there is a distortion process which does not create ordered structures. This is most clearly seen at the left part of the interface in Figure 7b. Thus the formation of lamellae is not an equilibrium morphology. They are only stable for a certain time interval because the thermal annealing was carried out very close to the T_g of PPE. Disordered micelles of SEBS in the PPE matrix should be the final state.

Some more details can be observed at the interface of SEBS with i-PP as shown in Figure 8. Three different areas at the SEBS/i-PP interface are shown after isothermal annealing for 2 h at 165 °C. The first process shown in Figure 8a is an rearrangement of the cylinders at the i-PP interface. The left side of the TEM micrograph shows the PS cylinders of SEBS and the right side is the i-PP phase. Obviously the PS cylinders of SEBS arrange parallel to the interface as already discussed for the system SEBS/PPE. The driving force for this process is similar to that of the previous case. Here it is the miscibility between i-PP and the EB matrix as well as the corresponding repulsion between PS cylinders and i-PP.[11] Arranging the cylinders parallel to the interface provides the initial opportunity to avoid the contact between i-PP and PS cylinders of SEBS. Figure 8b shows that the rearrangement process takes place for several layers of cylinders. This might be caused by the fact that the two PS blocks of one chain belong preferentially to two different PS cylinders. This argument is also used for the explanation of the better ordering behavior of a PS/PVP triblock copolymer with cylindrical morphology in contrast to the respective diblock copolymer.[7] Finally, the cylinders are arranged as schematically shown in Figure 8d. Another process also schematically shown in Figure 8d and experimentally observed in Figure 8c is the dissolution of the crystallographic arrangement of microdomains in the block copolymer. Separate micelles diffuse then into the i-PP bulk phase. The driving force for this process is also the miscibility of the EB block with i-PP.

It is now interesting to study if the morphology development at the interface correlates with the adhesion strength of SEBS with a-PS, PPE, and i-PP. Figure 9 shows some typical peel test results of bilayer specimens of SEBS with a-PS or PPE. For short annealing times both bilayer specimens have a similar weak adhesion at the interface. For the system SEBS/a-PS the interface remains very weak, which is in agreement with the TEM measurements discussed above. As also discussed above, there is only a contact of one PS lamella of the block copolymer with the a-PS hompolymer. Additionally the molecular weight of the PS blocks (12 600) is below the entanglement molecular weight of polystyrene.[21] Thus the interfacial strength is not significantly reinforced as demonstrated for different systems.[22] In contrast the peel strength increases very much for the system SEBS / PPE which is most pronounced after an annealing time of 24 h at 225 °C. Here the miscibility between the PS block and PPE is responsible for the increase of the delamination force. Finally, Figure 10 summarizes all results of the peel tests. The interface between SEBS and a-PS remains weak for all annealing times employed. The interfacial strength between SEBS and PPE as well as i-PP increases significantly with annealing time. All results are in agreement with morphological observations made by TEM. It should be mentioned that kinetics of the increase of the peel strength with annealing time are not comparable because the annealing procedures are carried out at different temperatures. At 225 °C, which is just above the T_g of PPE, it is impossible to anneal the bilayer specimen of SEBS/i-PP because i-PP is too fluid and cannot be kept in the mold.

Conclusions

It has been shown that SAXS and TEM measurements lead to consistent results concerning the morphology of a microphase-separated SEBS block copolymer in bulk. Furthermore, TEM is a powerful tool that can be used in order to study the ordering behavior and interfacial transitions of SEBS at interfaces to various polymers. Peel tests of bilayer specimens of SEBS with a-PS, i-PP, or PPE can be correlated with the morphology at the interface revealed by TEM.

Acknowledgment. We wish to thank Prof. W. Probst, LEO, Oberkochen, Germany, for the use of the LEO 912 Omega apparatus.

References and Notes

(1) Holden, G.; Legge, N. R. In *Thermoplastic Elastomers*; Legge, N. R., Holden, G., Schroeder, H. E., Eds., Hanser Pub.: Munich, Germany 1987.
(2) Modic, M. J.; Pottick, L. A. *Polym. Eng. Sci.* **1993**, *33*, 819.
(3) Aggarwal, S. L. *Polymer* **1976**, *17*, 938.

(4) Xie, R.; Sun, G.; Yang, B.; Jiang, B. *Macromolecules* **1994**, *27*, 3444.
(5) Lodge, T. P.; Muthukumar, M. *J. Phys. Chem.* **1996**, *100*, 13275.
(6) Krausch, G. *Mat. Sci. Eng., Rep.* **1995**, *R14*, 1.
(7) Liu, Y.; Zhao, W.; Zheng, X.; King, A.; Singh, A.; Rafailovich, M. H.; Sokolov, J.; Dai, K. H.; Kramer, E. J.; Schwarz, S. A.; Gebizlioglu, O.; Sinha, S. K. *Macromolecules* **1994**, *27*, 4000.
(8) Shull, K. R. *Macromolecules* **1993**, *26*, 2346.
(9) Strobl, G. *Acta Crystallogr.* **1970**, *A26*, 367.
(10) Heckmann, W. *Proc. Int. Congr. Electron. Microsc., XIIth* **1990**, *4*, 854.
(11) Setz, S.; Stricker, F.; Kressler, J.; Duschek, T.; Mülhaupt, R. *J. Appl. Poym. Sci.* **1996**, 59, 1117.
(12) Koberstein, J.; Russell, T.; Walsh, D.; Pottick, L. *Macromolecules* **1990,** *23*, 877.
(13) Schwab, M.; Stühn, B. *Phys. Rev. Lett.* **1996**, 76, 924.
(14) Mittelbach, P.; Porod, G. *Acta Phys. Austriaca* **1961,** *14*, 405.
(15) Hashimoto, T.; Kawamura, T.; Harada, M.; Tanaka, H. *Macromolecules* **1994**, *27*, 3063.
(16) Winey, K. I.; Gobran, D. A.; Xu, Z. D.; Fetters, L. J.; Thomas, E. L. *Macromolecules* **1994**, *27*, 2392.
(17) Kambour, R. P.; Bendler, J. T.; Bopp, C. R. *Macromolecules* **1983**, *16*, 753.
(18) Tucker, P. S.; Barlow, J. W.; Paul, D. R. *Macromolecules* **1988**, *21*, 1022.
(19) Kressler, J.; Kammer, H. W.; Morgenstern, U.; Litauszki, B.; Berger, W.; Karasz, F. E. *Makromol. Chem.* **1990**, *191*, 243.
(20) Chiu, H.-T.; Hwung, D.-S. *Eur. Polym. J.* **1994**, *30*, 1191.
(21) Ferry, J. D. *Viscoelastic Properties of Polymers*, 3rd ed.; John Wiley & Sons: New York, 1980.
(22) Creton, C.; Kramer, E. J.; Hui, C.-Y.; Brown, H. R. *Macromolecules* **1992**, *25*, 3075.

MA9617072